iScience

CellPress

Article

Chemical Environment-Induced Mixed Conductivity of Titanate as a Highly Stable Oxygen Transport Membrane

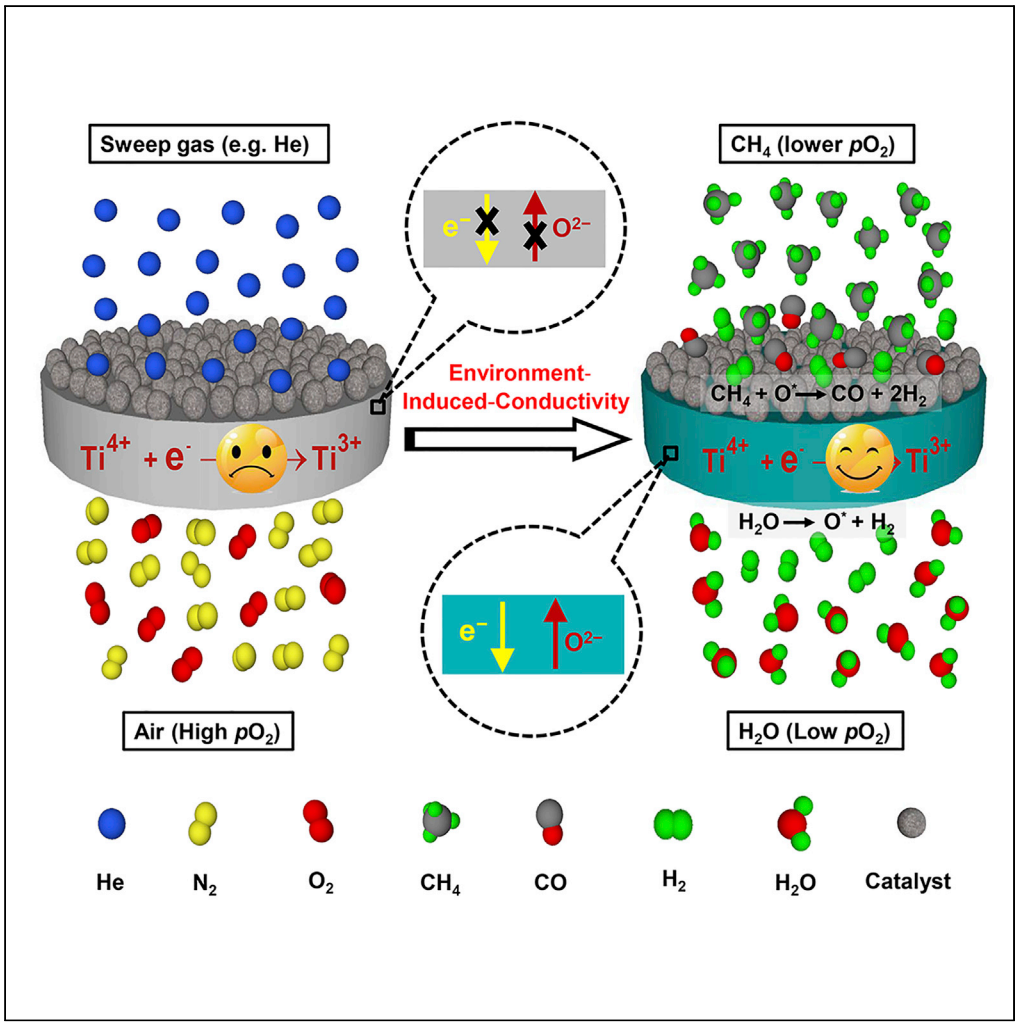

Guanghu He, Wenyuan Liang, Chih-Long Tsai, Xiaoliang Xia, Stefan Baumann, Heqing Jiang, Wilhelm Albert Meulenberg

jianghq@qibebt.ac.cn

HIGHLIGHTS

A new both Co- and Fe-free titanate-based oxygen transport membrane is developed

The membrane exhibits superior reduction tolerance in 20 vol.% H_2/Ar

The membrane shows an environment-induced mixed conductivity

The material is well suited for membrane reactor for coupling two reactions

He et al., iScience *19*, 955–964 September 27, 2019 © 2019 The Authors.
https://doi.org/10.1016/j.isci.2019.08.032

iScience

CellPress

Article

Chemical Environment-Induced Mixed Conductivity of Titanate as a Highly Stable Oxygen Transport Membrane

Guanghu He,[1,2] Wenyuan Liang,[1,3] Chih-Long Tsai,[2] Xiaoliang Xia,[1] Stefan Baumann,[2] Heqing Jiang,[1,3,5,*] and Wilhelm Albert Meulenberg[2,4]

SUMMARY

Coupling of two oxygen-involved reactions at the opposite sides of an oxygen transport membrane (OTM) has demonstrated great potential for process intensification. However, the current cobalt- or iron-containing OTMs suffer from poor reduction tolerance, which are incompetent for membrane reactor working in low oxygen partial pressure (pO_2). Here, we report for the first time a both Co- and Fe-free $SrMg_{0.15}Zr_{0.05}Ti_{0.8}O_{3-\delta}$ (SMZ-Ti) membrane that exhibits both superior reduction tolerance for 100 h in 20 vol.% H_2/Ar and environment-induced mixed conductivity due to the modest reduction of Ti4+ to Ti3+ in low pO_2. We further demonstrate that SMZ-Ti is ideally suited for membrane reactor where water splitting is coupled with methane reforming at the opposite sides to simultaneously obtain hydrogen and synthesis gas. These results extend the scope of mixed conducting materials to include titanates and open up new avenues for the design of chemically stable membrane materials for high-performance membrane reactors.

INTRODUCTION

Process intensification based on catalytic membrane reactors (CMRs) combing catalytic reactions and separation processes in one single unit presents one of the most important trends in today's chemical engineering and process technology (Morejudo et al., 2016; Tou et al., 2017). As one of the typical inorganic membranes for CMRs, dense oxygen transport membranes (OTMs) with mixed ionic-electronic conductivity (Wang et al., 2005a, 2005b) exhibit high oxygen ion permeability and infinite selectivity at elevated temperatures because of mobile oxygen vacancies and electronic defects. These features enable an OTM to simultaneously combine oxygen-related chemical reactions at two opposite sides of the membrane, leading to an integral coupling of reaction-separation-reaction processes and, hence, benefit with regard to energy consumption, capital cost, and catalytic performance. These benefits of OTM reactor have been demonstrated in our previous works (Jiang et al., 2008; Jiang et al., 2009a, 2009b; Jiang et al., 2010a, 2010b). For example, water splitting was coupled with partial oxidation of methane (POM) using a $BaCo_xFe_yZr_{1-x-y}O_{3-\delta}$ membrane (Jiang et al., 2008). At one side of the membrane, hydrogen is obtained from water splitting; meanwhile, at the other side, POM reaction occurs to produce synthesis gas with a H_2/CO ratio of around 2, which is proper for the subsequent Fischer-Tropsch or methanol production. In addition, some other researchers combine two oxygen-involved reactions at the opposite sides of OTM reactors for two synthesis gases (i.e., H_2/N_2 and H_2/CO) production for ammonia and liquid fuel (Li et al., 2016), large-scale hydrogen production (Fang et al., 2016; Li et al., 2017), or CO_2 capture and utilization (Kathiraser et al., 2013; Zhang et al., 2014), further underscoring the promise of OTM reactors for coupling two reactions on the opposite sides.

In spite of these advantages, distinct skepticism currently remains about the applicability of such reactors owing to the poor reduction tolerance of the existing OTM materials whose two sides are usually subjected to an oxygen-containing species (H_2O, NO_x) and a reductive gas (CH_4, C_2H_6), respectively. Conventional "first-generation" OTMs are based on cobalt perovskite oxides (e.g., $Ba_{0.5}Sr_{0.5}Co_{0.8}Fe_{0.2}O_{3-\delta}$) that exhibit high oxygen permeability and work well for air separation at relatively high oxygen partial pressure (pO_2) (Tan et al., 2008; Thursfield and Metcalfe, 2007), but the performance of Co-based membranes drops rapidly owing to the fast and deep reduction of cobalt ions followed by the eventual collapse of perovskite structure under low pO_2 environments in which two reactions are coupled at opposite sides of the membranes (Bouwmeester, 2003; Ovenstone et al., 2008). "Second-generation" OTMs, based on

[1]Qingdao Key Laboratory of Functional Membrane Material and Membrane Technology, Qingdao Institute of Bioenergy and Bioprocess Technology, Chinese Academy of Sciences, 266101 Qingdao, China

[2]Institute of Energy and Climate Research (IEK-1), Forschungszentrum Jülich GmbH, D-52425 Jülich, Germany

[3]University of Chinese Academy of Sciences, 100049 Beijing, China

[4]The University of Twente, Faculty of Science and Technology, Inorganic Membranes, 7500 AE Enschede, Netherlands

[5]Lead Contact

*Correspondence: jianghq@qibebt.ac.cn

https://doi.org/10.1016/j.isci.2019.08.032

This is an open access article under the CC BY-NC-ND license (http://creativecommons.org/licenses/by-nc-nd/4.0/).

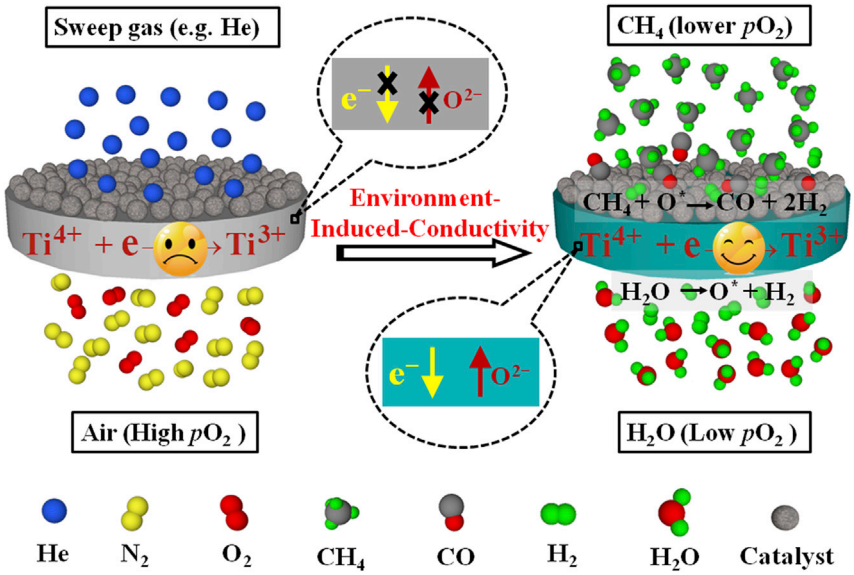

Scheme 1. The Exploitation of SMZ-Ti Mixed Conductivity Induced by Low pO_2 Environment and the Coupling of Water Splitting with Partial Oxidation of Methane Using an SMZ-Ti Membrane

iron-containing oxides such as $Ba_{0.5}Sr_{0.5}Fe_{0.8}Zn_{0.2}O_{3-\delta}$, $BaCe_xFe_{1-x}O_{3-\delta}$, and dual phase $Ce_{0.9}Gd_{0.1}O_{2-\delta}$ – $NiFe_2O_4$, exhibit relatively higher stability in low pO_2 than Co-based membrane (Luo et al., 2011; Wang et al., 2005a, 2005b; Zhu et al., 2006). Regrettably, performance degradation of Fe-based membranes cannot be avoided since the damage of Fe-based material is also inevitable (Neagu et al., 2013) when being used as reactor for coupling two chemical reactions under low pO_2. Hence, there is an urgent need to develop new membrane materials that allow the deployment of OTM reactors exhibiting desirable oxygen permeability as well as high chemical stability under low pO_2 atmospheres such as H_2O, CH_4, and H_2.

In this regard, titanates (e.g., $SrTiO_3$) are very intriguing materials because of the following considerations. (1) Titanates have excellent chemical and redox stability at high temperatures (Calle-Vallejo et al., 2010). (2) Under low pO_2 atmospheres, titanates show n-type conduction behaviors because of the reduction of Ti from 4+ to 3+ (Balachandran and Eror, 1981; Singh et al., 2013). Such reduction is compensated by the release of lattice oxygen from titanates to fulfill the electric neutrality and thereby forming oxygen vacancies (Balachandran and Eror, 1981; De Souza, 2015), enabling these titanates to possess mixed oxygen ionic-electronic conductivity for the applications in electrode for solid oxide fuel cells (SOFCs) (Ruiz-Morales et al., 2006) and electrocatalyst for metal-air batteries (Chen et al., 2015). (3) Furthermore, the ionic radii of Ti^{4+} and Ti^{3+} are comparable, which can avoid the large thermal and chemical expansions of titanates and ensure their mechanical and structural integrity under high temperature and reducing atmospheres. (4) The deep reduction of TiO_x to metallic state in H_2 is thermodynamically unfavorable (Neagu et al., 2013), suggesting superior chemical stability of titanates compared with cobalt- or iron-containing oxides (Calle-Vallejo et al., 2010). (5) Finally, B-site doping of Mg acceptor in titanates is helpful in creating more oxygen vacancies and lowering the sintering temperature (Li et al., 2014). Hence, the facts of the mixed ionic-electronic conductivity of titanates induced by low pO_2 environment and their superior chemical stability provide an opportunity to develop a new-generation titanate-based OTM reactor that is very suitable for coupling two oxygen-related reactions in low pO_2 environments.

Here, we first report a novel chemical environment-responsive mixed conducting $SrMg_{0.15}Zr_{0.05}Ti_{0.8}O_{3-\delta}$ (SMZ-Ti) oxygen transport membrane containing neither cobalt nor iron. With high valency and excellent anti-reduction properties, the Zr doping at the Ti-site of SMZ-Ti was used to dismiss the mismatch between cations for stabilizing the cubic structure. When being exposed to air as shown in Scheme 1, perovskite SMZ-Ti shows very poor mixed conductivity because the change of Ti valence from 4+ to 3+ is highly restricted under high pO_2 environment, and thus the Ti-based membrane shows negligible oxygen permeability under high pO_2 environment. Once both sides of the SMZ-Ti membrane are subjected to steam and

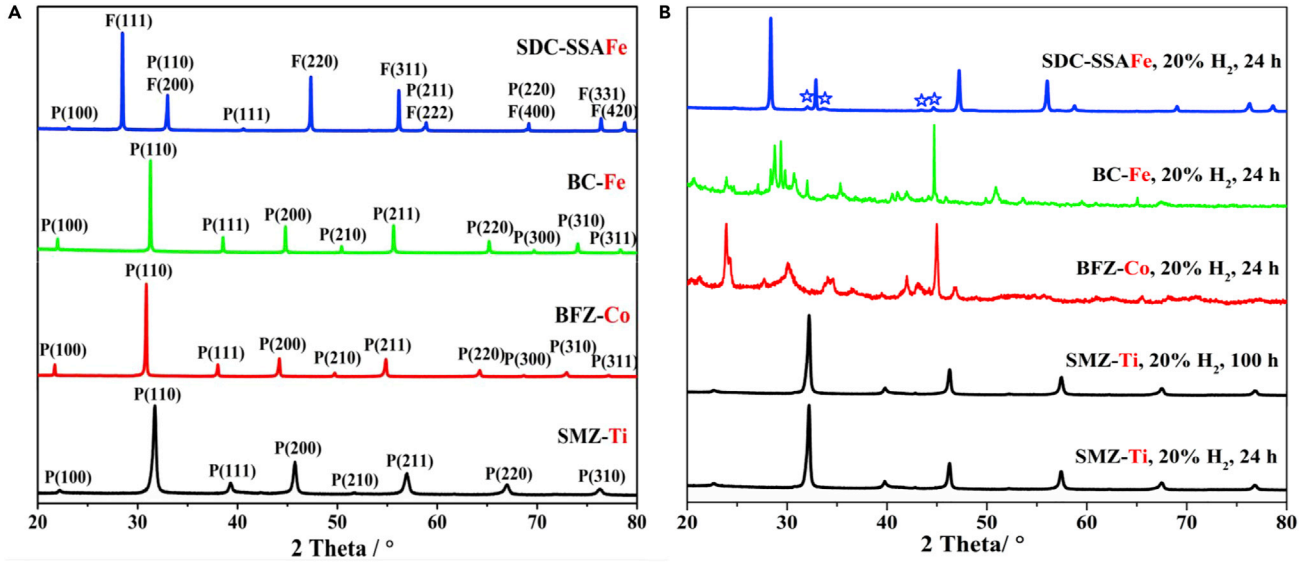

Figure 1. XRD Analyses of the Samples

(A) As-synthesized SMZ-Ti, BFZ-Co, BC-Fe, and SDC-SSAFe membrane materials at 950°C (see also Figure S2).

(B) H_2-exposed SMZ-Ti, BFZ-Co, BC-Fe, and SDC-SSAFe membrane materials at 900°C (see also Figure S1).

methane, respectively, these low pO_2 environments induce the release of lattice oxygen (O*) from SMZ-Ti, forming oxygen vacancies in the lattice, which are subsequently compensated by the modest reduction of Ti^{4+} to Ti^{3+} ($Ti^{4+} + e \rightarrow Ti^{3+}$). These oxygen vacancies and electronic defects induced by the chemical environment enable the dense SMZ-Ti membrane to show a mixed oxygen ionic-electronic conductivity and oxygen permeability, thus allowing the permeation of oxygen produced from water dissociation ($H_2O \rightarrow O^* + H_2$) on the membrane surface to the other side where it is consumed by POM to produce synthesis gas ($CH_4 + O^* \rightarrow CO + 2\ H_2$). Simultaneously, pure hydrogen as the product of water splitting is obtained. Apart from this chemical environment-induced mixed conductivity, SMZ-Ti also exhibits superior chemical stability under these low pO_2 atmospheres because the titanium ions (Ti^{4+}/Ti^{3+}) will not be deeply reduced to metallic state (Ti^0), contrasting with the well-known cobalt- or iron-containing membranes. Therefore, these features of SMZ-Ti dovetail exactly with OTM reactors to couple reaction-separation-reaction process, extend the scope of mixed conducting materials to include titanates, and open up new avenues for the design of promising chemically stable membrane materials for use in high-performance membrane reactors under harsh reaction conditions.

RESULTS AND DISCUSSION

Chemical Stability in Low pO_2 Atmospheres

As mentioned earlier, OTM reactors for practical application must exhibit excellent chemical resistance to reducing gases. When coupling two reactions in an OTM reactor, H_2 either is formed at the membrane surface by light hydrocarbon conversion process or exits on both sides of membrane. To evaluate the chemical stability against reducing atmosphere, SMZ-Ti membranes were treated in H_2 atmosphere, comparing with five typical Co- or Fe-containing OTMs, including $BaFe_{0.4}Zr_{0.2}Co_{0.4}O_{3-\delta}$ (BFZ-Co) (Jiang et al., 2010a, 2010b), $Ba_{0.98}Ce_{0.05}Fe_{0.95}O_{3-\delta}$ (BC-Fe) (Li et al., 2016), $Sm_{0.15}Ce_{0.85}O_{1.925}$ – $Sm_{0.6}Sr_{0.4}Al_{0.3}Fe_{0.7}O_{3-\delta}$ (SDC−SSAFe) (Fang et al., 2016; Li et al., 2017), $La_{0.9}Ca_{0.1}FeO_{3-\delta}$ (LC-Fe) (Wu et al., 2015), and $SrTi_{0.75}Fe_{0.25}O_{3-\delta}$ (ST-Fe) (Schulze-Küppers et al., 2015). Figures 1 and S1 depict the X-ray diffraction (XRD) patterns of SMZ-Ti, BFZ-Co, BC-Fe, SDC – SSAFe, LC-Fe, and ST-Fe membranes before and after H_2 treatment. As shown in Figure 1A, the as-synthesized SMZ-Ti membrane reveals a highly crystalline character, indexed as the cubic perovskite phase with space group *Pm-3m*. A weak peak at around 43° (2θ) could be assigned to MgO (Tkach et al., 2004). The structural evolution of $SrMg_xZr_{0.05}Ti_{0.95-x}O_{3-\delta}$ with varying Mg contents was investigated (Figure S2), and $SrMg_{0.15}Zr_{0.05}Ti_{0.8}O_{3-\delta}$ was selected for the following studies. After annealing in a 20 vol.% H_2/Ar atmosphere at 900°C for 24 h, the peaks in XRD pattern in Figure 1B of SMZ-Ti oxide associated with the cubic structure were still maintained, and no new phases were found even when the H_2-exposure period was extended to 100 h. In contrast, the cubic perovskite

structures of the conventional BFZ-Co, BC-Fe, LC-Fe, and ST-Fe membrane materials were decomposed seriously after exposure to 20 vol.% H_2/Ar atmosphere for 24 h (Figures 1B and S1). Similarly, after the same atmosphere exposure, a few impurity phases corresponding to $Sr_4Fe_6O_{13}$ (JCPDS no. 78-2403) and Fe metallic (JCPDS no. 87-0721) were also observed in the XRD pattern of the SDC−SSAFe membrane, indicating that this membrane material is still chemically unstable in the low oxygen partial pressure atmosphere. Thus, these chemical stability tests reveal that SMZ-Ti shows superior reduction-tolerant ability compared with the conventional Co- or Fe-containing membranes, which will assure the long-term operating durability of the SMZ-Ti membrane used as a membrane reactor working in reducing atmospheres.

Oxygen Permeability of SMZ-Ti under Different Working Conditions

Besides the superior chemical stability in low pO_2, another core requirement for new-generation OTMs is that the membrane should also possess a desirable oxygen permeability in low pO_2 environment. Therefore, the oxygen permeation flux of the SMZ-Ti membrane was investigated under four working conditions with different pO_2. The order of these working conditions for permeation measurement was Cond. I, Cond. II, Cond. III, and Cond. IV. As shown in Figure 2A, when one side of the membrane was fed with air while helium was swept on the other side (Cond. I), the oxygen permeation flux of the doped perovskite SMZ-Ti was about 0.02 $cm^3\ min^{-1}\ cm^{-2}$ at 990°C. This value is approximately one order of magnitude higher than that of undoped $SrTiO_3$ membrane exposed to air/argon pO_2 gradient at 1000°C (Schulze-Küppers et al., 2015), indicating the positive influence of Mg and/or Zr doping on oxygen permeability of $SrTiO_3$. This observation can be supported by the increased electrical conductivity and reduced activation energy for oxygen transport through Mg-doped $SrTiO_3$ as compared with undoped $SrTiO_3$ (Inoue et al., 1991; McColm and Irvine, 2001). However, the oxygen permeation flux of such titanate-based membrane is still too low under high pO_2 because of the presence of air. Once the helium sweep gas was changed to diluted hydrogen (Cond. II), the flux increased dramatically to over 0.1 $cm^3\ min^{-1}\ cm^{-2}$; continuously climbed up to 0.21 $cm^3\ min^{-1}\ cm^{-2}$ when both sides of the SMZ-Ti membrane were subjected to steam and methane, respectively (Cond. III); and even reached a value of 0.56 $cm^3\ min^{-1}\ cm^{-2}$ after introducing some CO_2 into the CH_4 stream (Cond. IV) to form much lower pO_2 at the methane side owing to the DRM reaction ($CH_4+CO_2 \rightarrow 2CO+2H_2$). These distinct differences in oxygen permeation flux of the SMZ-Ti membrane exposed to the above-mentioned four conditions show that pO_2 is strongly associated with oxygen permeability of SMZ-Ti.

To gain insight into the relationship between the pO_2 and oxygen permeability of SMZ-Ti, we performed equilibrium pO_2 calculation based on the gas components on the opposite sites of the SMZ-Ti membrane at 1 atm and 990°C using Gibbs free energy minimization algorithm on HSC Chemistry 5.0 software (Table S1), the same method as previous studies on the thermodynamic equilibrium for H_2O splitting and DRM (Furler et al., 2012; Gardner et al., 2013). As shown in Figure 2B, the pO_2 at the two sides of the SMZ-Ti membrane decreases from $10^{-0.7}/10^{-3.2}$ atm at Cond. I to $10^{-9.5}/10^{-18.4}$ atm at Cond. IV, corresponding to the gradual increase in oxygen permeation flux presented in Figure 2A. Compared with the pO_2 at permeate side under Cond. I, a much lower pO_2 of $10^{-15.7}$ atm under Cond. II is obtained because of the hydrogen gas, which facilitates the formation of electronic defects and oxygen vacancies in SMZ-Ti due to the reduction of Ti^{4+} to Ti^{3+}, as well as a larger gradient of pO_2 across the membrane as driving force, and thereby yields a higher permeation flux of 0.13 $cm^3\ min^{-1}\ cm^{-2}$. This environment-responsive mixed conductivity of SMZ-Ti is further verified by the increase of oxygen permeation flux of the SMZ-Ti membrane when BOTH sides of the membrane are exposed to H_2O and CH_4 or H_2O and CH_4-CO_2 atmospheres with lower pO_2 (Cond. III and Cond. IV), respectively, even though the pO_2 gradient across the membrane in either cases is slightly smaller than that for air/He-H_2 gradient (Cond. II). Basically, the pO_2 calculated by HSC Chemistry represents an overall average equilibrium amount of oxygen in a whole system. However, if a series of chemical reactions takes place sequentially in the system, the involved components will be unevenly distributed and thus lead to a pO_2 gradient throughout the catalyst bed (Chen et al., 2018). In the case of Cond. IV in the present work, a series of catalytic reforming and syngas oxidation reactions occurs at the permeate side of the SMZ-Ti membrane (Figure S3). The CO and H_2 produced from dry reforming of CH_4 with CO_2 at the top zone of catalyst bed can reach the near SMZ-Ti surface and further consume the permeated oxygen species, thus obtaining the highest environment-induced mixed conductivity and oxygen permeation flux. It is necessary to point out that the thickness of the SMZ-Ti membrane used here is 0.7 mm, which means that the permeation flux can be improved by shaping the material into hollow fiber configuration membrane with thin dense layer and larger effective area. Also, the rate-controlling step

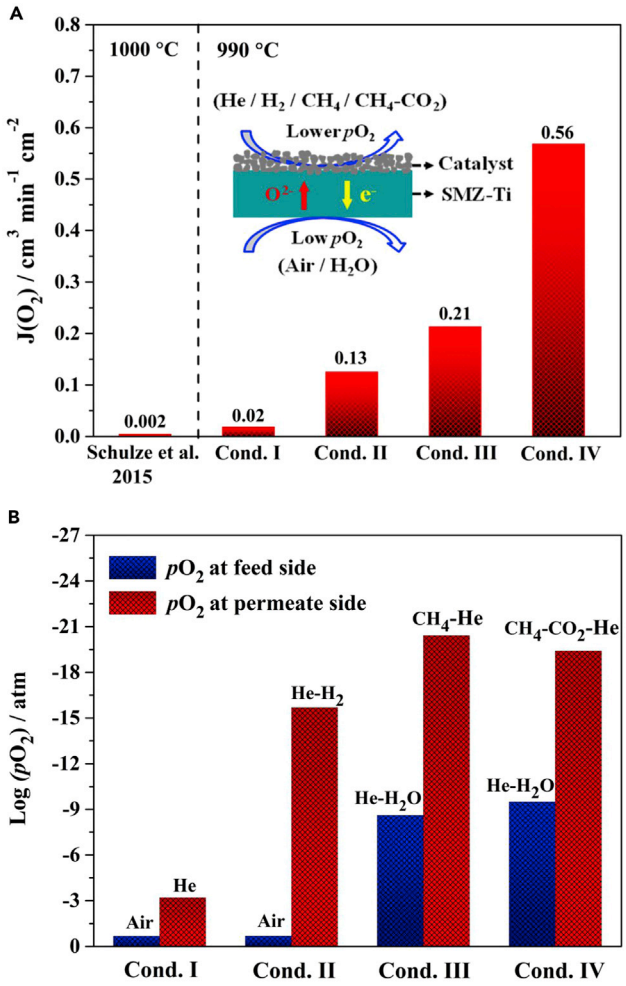

Figure 2. Oxygen Permeability of SMZ-Ti Membrane

Oxygen permeation flux (A) and pO_2 at the two sides (B) of SMZ-Ti membranes at 990°C under four different operating conditions (see also Figure S3 and Table S1).

(Cond. I) F_{Air} = 60 cm^3 min^{-1}; F_{He} = 20 cm^3 min^{-1}.

(Cond. II) F_{Air} = 15 cm^3 min^{-1}; F_{H2} = 5 cm^3 min^{-1} diluted by 15 cm^3 min^{-1} of helium.

(Cond. III) F_{H2O} = 30 cm^3 min^{-1} carried by 10 cm^3 min^{-1} of helium; F_{CH4} = 3 cm^3 min^{-1} diluted by 13 cm^3 min^{-1} of helium, 4 cm^3 min^{-1} of N_2 as internal standard gas.

(Cond. IV) F_{H2O} = 30 cm^3 min^{-1} carried by 10 cm^3 min^{-1} of helium; F_{CH4} = 3 cm^3 min^{-1}, F_{CO2} = 1.5 cm^3 min^{-1} diluted by 11.5 cm^3 min^{-1} of helium, 4 cm^3 min^{-1} of N_2 as internal standard gas.

in this H_2O splitting-oxygen separation-catalytic reforming process will be determined in the future, and further enhanced oxygen permeation flux can be expected. Obviously, the oxygen permeation flux of the SMZ-Ti membrane is obviously increasing with decreasing pO_2, even though the driving force between feed and permeate sides decreases in particular from Cond. II to Cond. III, which likely results from the chemical environment-induced mixed conductivity of SMZ-Ti. This feature finely matches the working environment of OTM reactor for coupling two reactions.

Electrical Conductivity of SMZ-Ti under Low pO_2 Atmospheres

The environment-induced mixed conductivity of the SMZ-Ti membrane can be also validated from the point of the electrical conductivity under different pO_2 atmospheres. For this purpose, electrochemical impedance spectra measurements were performed to investigate the electrical conduction behavior of SMZ-Ti. The Nyquist plots of AC impedance measurements of SMZ-Ti under different pO_2 at 900°C are shown in Figure 3A. The oxygen partial pressure was controlled by means of Ar-H_2-H_2O gas mixtures, which are similar to water splitting

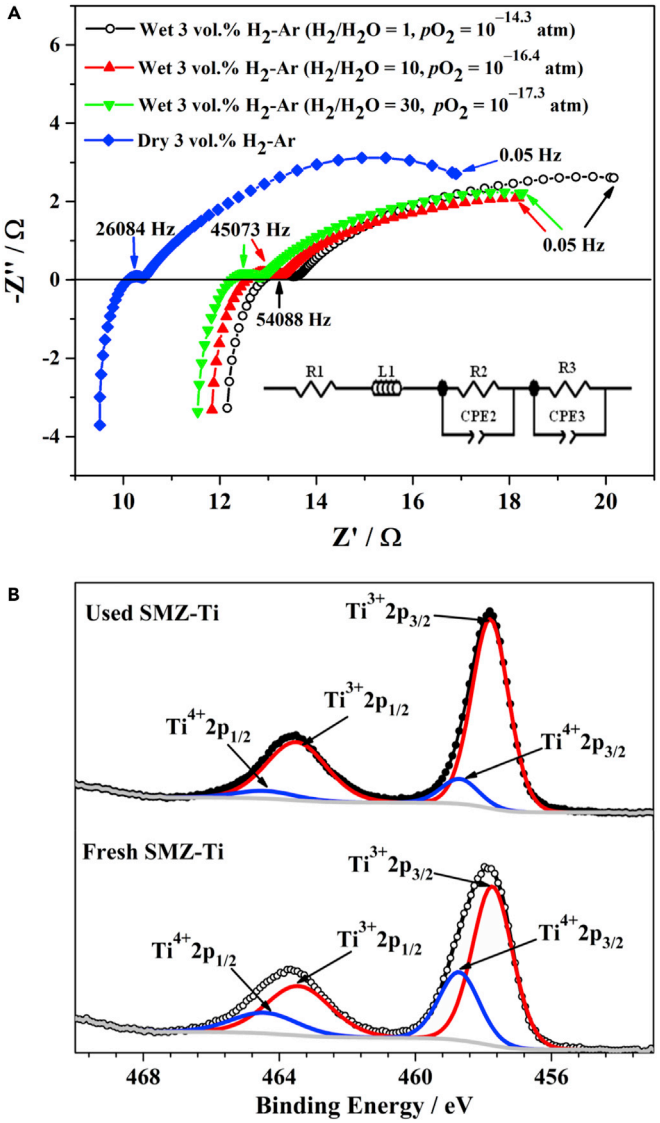

Figure 3. Electrical Conductivity and XPS Characterization of SMZ-Ti Sample

(A) AC impedance spectroscopy of Pt/SMZ-Ti/Pt as a function of oxygen partial pressure at 900°C, the pO_2 was also calculated using HSC Chemistry 5.0 software.

(B) Ti *2p* XPS spectra from the fractured surface of the SMZ-Ti sample before and after AC impedance measurement.

condition as shown in Figure 1. The typical stabilization time for each impedance measurement condition was over 50 h. A model circuit was used for simulating the impedance data as shown in the inset of Figure 3A, where R is a resistance, L is an inductance, and CPE is a constant phase element. From the simulation results, R1 can be assigned as total resistance across the measured sample, L1 is the inductance from the system setup, R2/CPE2 represents the contact resistance in between sample and electrode and R3/CPE3 is the electrochemical reaction for gas exchange in between sample and atmosphere (Irvine et al., 1990). Based on the Nyquist plots and the model circuit, the electrical conductivity of SMZ-Ti increases gradually with decreasing pO_2 according to the H_2/H_2O mole ratio, showing an n-type conduction behavior. In particular, the resistance of SMZ-Ti under dry 3 vol.% H_2/Ar atmosphere was approximately 10 Ω and thereby the electrical conductivity in this case was ~0.1 S/cm. This value is basically in agreement with the conductivity of $SrTiO_3$ in previous studies (Balachandran and Eror, 1981; Inoue et al., 1991).

After nearly 300 h of the impedance measurement at low pO_2 atmospheres, the chemical state of Ti ions in the spent SMZ-Ti sample was studied by X-ray photoelectron spectroscopy (XPS) analysis to

compare with the results of the sample before impedance measurement. As shown in Figure 3B, the peaks of the fresh SMZ-Ti sample located at binding energies 458.7 eV (Ti $2p_{3/2}$) and 464.4 eV (Ti $2p_{1/2}$) are ascribed to Ti^{4+} in perovskite lattice (Bharti et al., 2016). The Ti 2p shoulder peaks at binding energy 457.7 eV (Ti $2p_{3/2}$) and 463.4 eV (Ti $2p_{1/2}$) are corresponding to Ti^{3+} (Wang et al., 2011), which is related to the intrinsic excitation of electrons from the valence bands of Ti^{4+} to the conduction bands by Mg^{2+} acceptor doping and thereby resulting in the reduction to Ti^{3+} to fulfill the electric neutrality criteria (Singh et al., 2013). After impedance measurement, the percentage of Ti^{3+} in Ti cations for the used SMZ-Ti sample increased significantly compared with the as-prepared sample, revealing the chemical reduction of Ti^{4+} ions in 3% H_2-Ar at 900°C. Also, it can be inferred that such environment-induced Ti^{4+} reduction will be further enhanced by decreasing the pO_2 (e.g. 50 vol.% H_2). In addition, no XPS peaks of Ti^{2+}, Ti^{+}, and metallic Ti^{0} species were observed in the used sample after this long-term exposure to low pO_2 atmospheres, indicating that no deep reduction occurred for Ti^{4+}/Ti^{3+} ions to cause cubic structure distortion. Accordingly, SMZ-Ti has superior reduction tolerance, which is again confirmed by the XRD patterns of the SMZ-Ti sample before and after impedance measurement (Figure S4).

The impedance spectra indicate that the electrical conductivity of SMZ-Ti increases by decreasing the pO_2, showing an n-type conduction behavior. Such behavior is related to the modest reduction of Ti^{4+} to Ti^{3+} in low pO_2 according to the XPS studies of SMZ-Ti sample before and after impedance measurement. Furthermore, this n-type conduction behavior of SMZ-Ti is in accordance with the observed oxygen permeation fluxes of the SMZ-Ti membrane under different working conditions as shown in Figure 2, which again confirms that lower pO_2 environment can induce the modest reduction of Ti^{4+} to Ti^{3+} in SMZ-Ti, allowing the SMZ-Ti membrane to possess higher mixed conductivity and better oxygen permeability.

Membrane Performance under Reaction Condition

After confirming that the SMZ-Ti membrane possesses superior chemical stability and good oxygen permeation flux under low pO_2, we then proceeded to evaluate SMZ-Ti membrane performance under harsh chemical reaction conditions. For this purpose, coupling of water splitting with dry reforming of methane is an ideal model process because it provides a good platform to investigate the tolerance of the SMZ-Ti membrane to harsh chemical environment, including CH_4, H_2, CO_2, and CO, especially CO_2, which is another main problem of many perovskite-type OTMs suffering from CO_2 erosion via carbonate formation (Yi et al., 2010; Zhang et al., 2017).

Following a 100-h operation at varying conditions, two sides of the SMZ-Ti membrane was then subjected to H_2O splitting and dry reforming of CH_4 (mole ratio of CH_4/CO_2 = 2), respectively, and continuously operated at constant condition for another 100 h, as shown in Figure 4A. Throughout this period, CH_4 conversion remained at about 72% without any fluctuations, CO selectivity was high (96%–97%), and at the opposite side the H_2 production rate stayed roughly at 1.1 $cm^3\ min^{-1}\ cm^{-2}$. These results indicate that SMZ-Ti was operated steadily when its two sides were subjected to the reaction conditions of water splitting coupled with dry reforming of methane. Noted that the CH_4 conversion in this case exceeds the equilibrium value of CH_4 conversion according to DRM reaction ($CH_4 + CO_2 \rightarrow 2CO + 2H_2$) calculated by HSC Chemistry 5.0 (Figure S5), suggesting that POM also takes place with DRM. The composition of the effluent stream at the permeate side as function of time was provided in Table S2. A typical gas composition of ~48% He, ~16.3% N_2, ~3.6% CH_4, ~17.2% H_2, ~14.9% CO, and a small amount of CO_2 implies that the possible H_2O and/or CO_2 formed at the membrane surface were finally converted with unreacted methane to syngas via reforming processes. The carbon balance at this side of the membrane maintained at over 96% within the investigation period. However, it is clear that the mole balance of carbon increased slowly with operating time, suggesting that slight carbon deposition may take place in the catalyst bed. This is confirmed by the thermogravimetric analysis of the Ni/Al_2O_3 catalyst after an approximately 200-h operation (Figure S6).

Both sides of the spent SMZ-Ti membrane were studied by scanning electron microscope (SEM)-energy-dispersive X-ray spectroscopy (EDXS). The same as the as-prepared SMZ-Ti membrane (Figure S7), the spent membrane was still intact and did not show any physical damage (Figures 4B and 4D). What is more, the Ti element (small white spots) at the two sides of the spent membrane was evenly distributed (Figures 4C and 4E). In contrast to the conventional cobalt-containing $Ba_{0.5}Sr_{0.5}Co_{0.8}Fe_{0.2}O_{3-\delta}$ (BSCF)

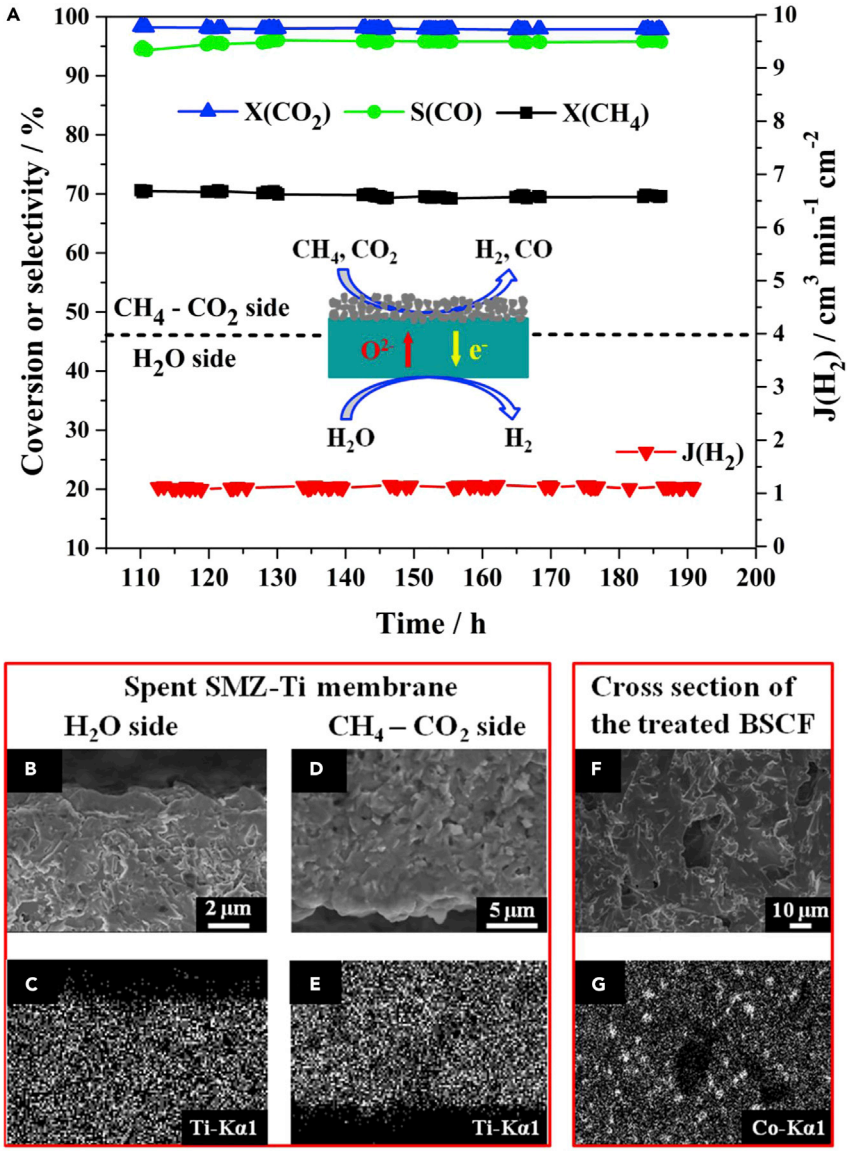

Figure 4. Membrane Performance of SMZ-Ti under Reaction Conditions

(A) Stable operation of the SMZ-Ti membrane reactor at 990°C. H_2O side: F_{H2O} = 30 cm^3 min^{-1}, F_{He} = 10 cm^3 min^{-1}; CH_4-CO_2 side: F_{total} = 20 cm^3 min^{-1} (F_{CH4} = 3 cm^3 min^{-1}, F_{CO2} = 1.5 cm^3 min^{-1}, F_{N2} = 4 cm^3 min^{-1}, F_{He} = 11.5 cm^3 min^{-1}).

(B and C) SEM-EDXS images of the H_2O side of the SMZ-Ti membrane after about 200 h operation.

(D and E) SEM-EDXS images of the CH_4-CO_2 side of the SMZ-Ti membrane after about 200 h operation.

(F and G) SEM-EDXS images of the cross section of the BSCF membrane after treatment at 900°C for 0.5 h in 2.5 vol.% H_2 – 75 vol.% H_2O-22.5% He atmosphere.

See also Table S2, Figures S5–S10.

membrane treated under simulated H_2O splitting condition for only 0.5 h, many small particles of 2–5 μm were observed on the cross section of the membrane (Figure 4F). EDXS results reveal that these particles mainly consisted of cobalt (Figure 4G), indicating that the cobalt ions in BSCF were reduced and exsolved from the perovskite lattice under such low pO_2 atmosphere. This is similar to the previous observations of the cobalt-based oxygen transport membrane (Jiang et al., 2010a, 2010b). The slight carbon enrichment at the CH_4-CO_2 side of the spent membrane (Figure S8) is probably due to a small amount of coke deposition and/or carbonate formation on the membrane surface. To examine the CO_2 tolerance of SMZ-Ti, the SMZ-Ti sample was subjected to annealing in 7.5 vol.% CO_2/He at 990°C for 24 h. The cubic structure of

CO_2-annealed SMZ-Ti remained unchanged, and no obvious carbonate formation was observed (Figure S9). This observation is in contrast with that for BSCF after exposure to CO_2 under the same condition. These results clearly demonstrate that SMZ-Ti had better CO_2 tolerance than BSCF. Compared with the as-prepared SMZ-Ti membrane, no obvious difference in the XRD patterns of the spent membrane except the strontium silicate diffraction peaks (due to commercial glass sealant used in this work) was found (Figure S10). Thus, all these results confirm that SMZ-Ti is a reduction-tolerant, CO_2-stable and high-permeability oxygen transport membrane, holding great promise for a new-generation membrane used as membrane reactors.

Conclusions

We report the first novel chemical environment-induced mixed conducting SMZ-Ti oxygen transport membrane (OTM) containing neither cobalt nor iron. Contrary to the well-known cobalt- or iron-containing membrane suffering from poor reduction tolerance, our results demonstrate that the novel SMZ-Ti membrane exhibits both excellent chemical stability for 100 h in 20 vol.% H_2/Ar and environment-induced mixed ionic-electronic conductivity due to the modest reduction of Ti4+ to Ti3+ in low pO_2. These features dovetail exactly with OTM reactors to couple two reactions under low pO_2, which was also highlighted by coupling water splitting with methane reforming at the opposite sides to simultaneously obtain pure hydrogen and synthesis gas. Our findings of a new class of mixed ionic-electronic conductor can extend the limited choice of OTM materials to include titanates and open up new avenues for the design of promising chemically stable membrane materials for use in high-performance membrane reactors toward green and sustainable chemistry.

Limitations of the Study

In this study, the thickness of the SMZ-Ti membrane used is 700 μm. So, hollow fiber configuration SMZ-Ti membranes with thin dense layer and larger effective area will be developed for further improving the permeation flux.

METHODS

All methods can be found in the accompanying Transparent Methods supplemental file.

SUPPLEMENTAL INFORMATION

Supplemental Information can be found online at https://doi.org/10.1016/j.isci.2019.08.032.

ACKNOWLEDGMENTS

This work was financially supported by the National Natural Science Foundation of China (21676284, 21506237), the International Partnership Program of the Chinese Academy of Sciences (Grant No. 153937KYSB20180048) and the Grant of DICP & QIBEBT UN201708. G.H. gratefully thanks the support via "Youth Innovation Promotion Association Chinese Academy of Sciences Grant 2018245." The authors thank Dr. Ivanova Mariya for her support on analyzing the AC impedance spectra. Support in XPS analysis by Dr. Heinrich Hartmann is acknowledged.

AUTHOR CONTRIBUTIONS

H.J. and G.H. conceived and designed the experiments. G.H. conducted the experiments and summarized the data. W.L. conducted the sample preparation. C.-L.T. performed the modeling of impedance spectra. X.X. undertook the treatment of BSCF sample. S.B. and W.A.M. assisted with the impedance measurement and sample annealing. H.J. supervised the whole work. H.J. and G.H. wrote the manuscript.

DECLARATION OF INTERESTS

The authors declare that they have no competing interests.

Received: February 21, 2019
Revised: June 30, 2019
Accepted: August 20, 2019
Published: September 27, 2019

REFERENCES

Balachandran, U., and Eror, N.G. (1981). Electrical conductivity in strontium titanate. J. Solid State Chem. *39*, 351–359.

Bharti, B., Kumar, S., Lee, H.N., and Kumar, R. (2016). Formation of oxygen vacancies and Ti^{3+} state in TiO_2 thin film and enhanced optical properties by air plasma treatment. Sci. Rep. *6*, 32355.

Bouwmeester, H.J.M. (2003). Dense ceramic membranes for methane conversion. Catal. Today *82*, 141–150.

Calle-Vallejo, F., Martínez, J.I., García-Lastra, J.M., Mogensen, M., and Rossmeisl, J. (2010). Trends in stability of perovskite oxides. Angew. Chem. Int. Ed. *49*, 7699–7701.

Chen, C.-F., King, G., Dickerson, R.M., Papin, P.A., Gupta, S., Kellogg, W.R., and Wu, G. (2015). Oxygen-deficient $BaTiO_{3-x}$ perovskite as an efficient bifunctional oxygen electrocatalyst. Nano Energy *13*, 423–432.

Chen, Y., de Glee, B., Tang, Y., Wang, Z., Zhao, B., Wei, Y., Zhang, L., Yoo, S., Pei, K., Kim, J.H., et al. (2018). A robust fuel cell operated on nearly dry methane at 500°C enabled by synergistic thermal catalysis and electrocatalysis. Nat. Energy *3*, 1042–1050.

De Souza, R.A. (2015). Oxygen diffusion in $SrTiO_3$ and related perovskite oxides. Adv. Funct. Mater. *25*, 6326–6342.

Fang, W., Steinbach, F., Cao, Z., Zhu, X., and Feldhoff, A. (2016). A highly efficient sandwich-like symmetrical dual-phase oxygen-transporting membrane reactor for hydrogen production by water splitting. Angew. Chem. Int. Ed. *128*, 8790–8793.

Furler, P., Scheffe, J.R., and Steinfeld, A. (2012). Syngas production by simultaneous splitting of H_2O and CO_2 via ceria redox reactions in a high-temperature solar reactor. Energy Environ. Sci. *5*, 6098–6103.

Gardner, T.H., Spivey, J.J., Kugler, E.L., and Pakhare, D. (2013). CH_4–CO_2 reforming over Ni-substituted barium hexaaluminate catalysts. Appl. Catal. A Gen. *455*, 129–136.

Inoue, T., Seki, N., Kamimae, J.-i., Eguchi, K., and Arai, H. (1991). The conduction mechanism and defect structure of acceptor- and donor-doped $SrTiO_3$. Solid State Ionics *48*, 283–288.

Irvine, J.T.S., Sinclair, D.C., and West, A.R. (1990). Electroceramics: characterization by impedance spectroscopy. Adv. Mater. *2*, 132–138.

Jiang, H., Cao, Z., Schirrmeister, S., Schiestel, T., and Caro, J. (2010a). A coupling strategy to produce hydrogen and ethylene in a membrane reactor. Angew. Chem. Int. Ed. *49*, 5656–5660.

Jiang, H., Liang, F., Czuprat, O., Efimov, K., Feldhoff, A., Schirrmeister, S., Schiestel, T., Wang, H., and Caro, J. (2010b). Hydrogen production by water dissociation in surface-modified $BaCo_xFe_yZr_{1-x-y}O_{3-\delta}$ hollow-fiber membrane reactor with improved oxygen permeation. Chem. Eur. J. *16*, 7898–7903.

Jiang, H., Wang, H., Liang, F., Werth, S., Schiestel, T., and Caro, J. (2009a). Direct decomposition of nitrous oxide to nitrogen by in situ oxygen removal with a perovskite membrane. Angew. Chem. Int. Ed. *48*, 2983–2986.

Jiang, H., Xing, L., Czuprat, O., Wang, H., Schirrnieister, S., Schiestel, T., and Caro, J. (2009b). Highly effective NO decomposition by in situ removal of inhibitor oxygen using an oxygen transporting membrane. Chem. Commun. 6738–6740.

Jiang, H., Wang, H., Werth, S., Schiestel, T., and Caro, J. (2008). Simultaneous production of hydrogen and synthesis gas by combining water splitting with partial oxidation of methane in a hollow-fiber membrane reactor. Angew. Chem. Int. Ed. *47*, 9341–9344.

Kathiraser, Y., Wang, Z., and Kawi, S. (2013). Oxidative CO_2 reforming of methane in $La_{0.6}Sr_{0.4}Co_{0.8}Ga_{0.2}O_{3-\delta}$ (LSCG) hollow fiber membrane reactor. Environ. Sci. Technol. *47*, 14510–14517.

Li, M., Pietrowski, M.J., De Souza, R.A., Zhang, H., Reaney, I.M., Cook, S.N., Kilner, J.A., and Sinclair, D.C. (2014). A family of oxide ion conductors based on the ferroelectric perovskite $Na_{0.5}Bi_{0.5}TiO_3$. Nat. Mater. *13*, 31–35.

Li, W., Cao, Z., Cai, L., Zhang, L., Zhu, X., and Yang, W. (2017). H_2S-tolerant oxygen-permeable ceramic membranes for hydrogen separation with a performance comparable to those of palladium-based membranes. Energy Environ. Sci. *10*, 101–106.

Li, W., Zhu, X., Chen, S., and Yang, W. (2016). Integration of nine steps into one membrane reactor to produce synthesis gases for ammonia and liquid fuel. Angew. Chem. Int. Ed. *55*, 8566–8570.

Luo, H., Efimov, K., Jiang, H., Feldhoff, A., Wang, H., and Caro, J. (2011). CO_2-stable and cobalt-free dual-phase membrane for oxygen separation. Angew. Chem. Int. Ed. *50*, 759–763.

McColm, T.D., and Irvine, J.T.S. (2001). B site doped strontium titanate as a potential SOFC substrate. Ionics *7*, 116–121.

Morejudo, S.H., Zanón, R., Escolástico, S., Yuste-Tirados, I., Malerød-Fjeld, H., Vestre, P.K., Coors, W.G., Martínez, A., Norby, T., Serra, J.M., and Kjølseth, C. (2016). Direct conversion of methane to aromatics in a catalytic co-ionic membrane reactor. Science *353*, 563–566.

Neagu, D., Tsekouras, G., Miller, D.N., Ménard, H., and Irvine, J.T.S. (2013). In situ growth of nanoparticles through control of non-stoichiometry. Nat. Chem. *5*, 916–923.

Ovenstone, J., White, J.S., and Misture, S.T. (2008). Phase transitions and phase decomposition of $La_{1-x}Sr_xCoO_{3-\delta}$ in low oxygen partial pressures. J. Power Sources *181*, 56–61.

Ruiz-Morales, J.C., Canales-Vázquez, J., Savaniu, C., Marrero-López, D., Zhou, W., and Irvine, J.T.S. (2006). Disruption of extended defects in solid oxide fuel cell anodes for methane oxidation. Nature *439*, 568–571.

Schulze-Küppers, F., ten Donkelaar, S.F.P., Baumann, S., Prigorodov, P., Sohn, Y.J., Bouwmeester, H.J.M., Meulenberg, W.A., and Guillon, O. (2015). Structural and functional properties of $SrTi_{1-x}Fe_xO_{3-\delta}$ ($0 \leq x \leq 1$) for the use as oxygen transport membrane. Sep. Purif. Technol. *147*, 414–421.

Singh, K., Nowotny, J., and Thangadurai, V. (2013). Amphoteric oxide semiconductors for energy conversion devices: a tutorial review. Chem. Soc. Rev. *42*, 1961–1972.

Tan, X., Pang, Z., and Li, K. (2008). Oxygen production using $La_{0.6}Sr_{0.4}Co_{0.2}Fe_{0.8}O_{3-\alpha}$ (LSCF) perovskite hollow fibre membrane modules. J. Membr. Sci. *310*, 550–556.

Thursfield, A., and Metcalfe, I.S. (2007). Air separation using a catalytically modified mixed conducting ceramic hollow fibre membrane module. J. Membr. Sci. *288*, 175–187.

Tkach, A., Vilarinho, P.M., and Kholkin, A. (2004). Effect of Mg doping on the structural and dielectric properties of strontium titanate ceramics. Appl. Phys. A *79*, 2013–2020.

Tou, M., Michalsky, R., and Steinfeld, A. (2017). Solar-driven thermochemical splitting of CO_2 and in situ separation of CO and O_2 across a ceria redox membrane reactor. Joule *1*, 146–154.

Wang, H., Tablet, C., Feldhoff, A., and Caro, J. (2005a). A cobalt-free oxygen-permeable membrane based on the perovskite-type oxide $Ba_{0.5}Sr_{0.5}Zn_{0.2}Fe_{0.8}O_{3-\delta}$. Adv. Mater. *17*, 1785–1788.

Wang, H., Werth, S., Schiestel, T., and Caro, J. (2005b). Perovskite hollow-fiber membranes for the production of oxygen-enriched air. Angew. Chem. Int. Ed. *44*, 6906–6909.

Wang, Z., Yang, F., Zhang, Z., Tang, Y., Feng, J., Wu, K., Guo, Q., and Guo, J. (2011). Evolution of the surface structures on $SrTiO_3$ (110) tuned by Ti or Sr concentration. Phys. Rev. B *83*, 155453.

Wu, X.-Y., Chang, L., Uddi, M., Kirchen, P., and Ghoniem, A.F. (2015). Toward enhanced hydrogen generation from water using oxygen permeating LCF membranes. Phys. Chem. Chem. Phys. *17*, 10093–10107.

Yi, J.X., Schroeder, M., Weirich, T., and Mayer, J. (2010). Behavior of Ba(Co, Fe, Nb)$O_{3-delta}$ perovskite in CO_2-containing atmospheres: degradation mechanism and materials design. Chem. Mater. *22*, 6246–6253.

Zhang, C., Sunarso, J., and Liu, S. (2017). Designing CO_2-resistant oxygen-selective mixed ionic–electronic conducting membranes: guidelines, recent advances, and forward directions. Chem. Soc. Rev. *46*, 2941–3005.

Zhang, K., Zhang, G., Liu, Z., Zhu, J., Zhu, N., and Jin, W. (2014). Enhanced stability of membrane reactor for thermal decomposition of CO_2 via porous-dense-porous triple-layer composite membrane. J. Membr. Sci. *471*, 9–15.

Zhu, X., Wang, H., and Yang, W. (2006). Structural stability and oxygen permeability of cerium lightly doped $BaFeO_{3-\delta}$ ceramic membranes. Solid State Ionics *177*, 2917–2921.

ISCI, Volume *19*

Supplemental Information

Chemical Environment-Induced Mixed Conductivity of Titanate as a Highly Stable Oxygen Transport Membrane

Guanghu He, Wenyuan Liang, Chih-Long Tsai, Xiaoliang Xia, Stefan Baumann, Heqing Jiang, and Wilhelm Albert Meulenberg

Supplemental Information

Supporting Figures

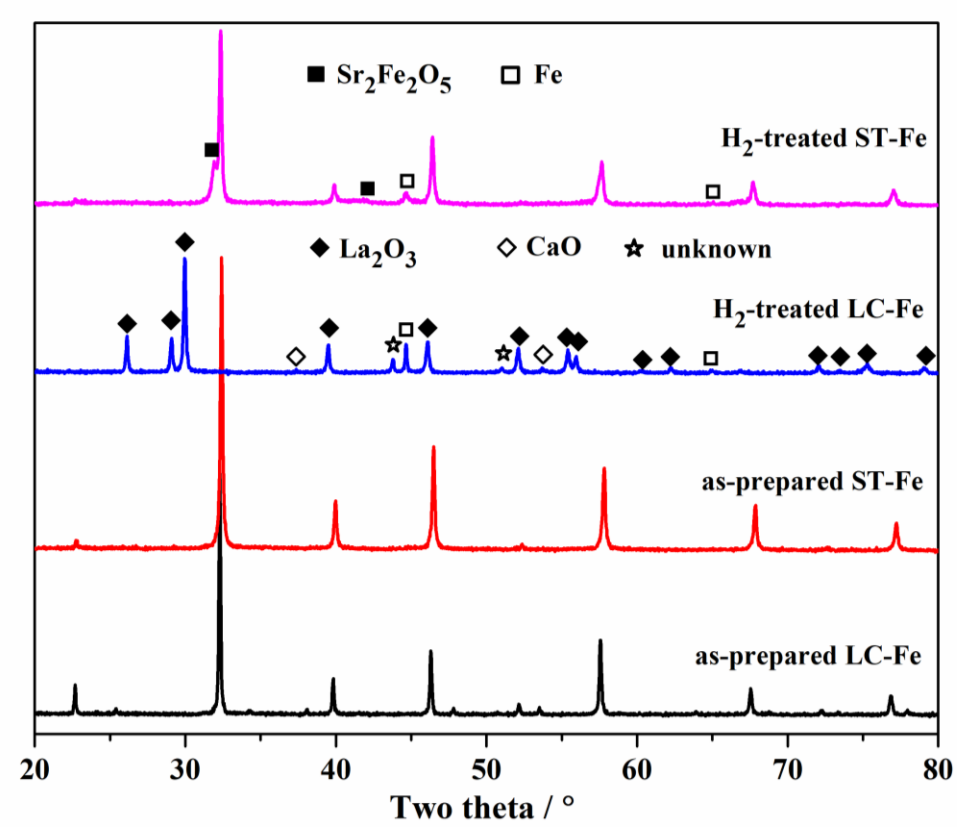

Figure S1. XRD patterns of LC-Fe and ST-Fe membrane materials before and after annealing in 20 vol.% H_2/Ar at 900 ℃ for 24 h. (Related to Figure 1b)

As shown in Figure S1, the cubic perovskite structures of the conventional LC-Fe and ST-Fe membrane materials were decomposed seriously after exposure to 20 vol.% H_2/Ar atmosphere for 24 h, indicating the poor chemical stability under reducing atmospheres relative to SMZ-Ti.

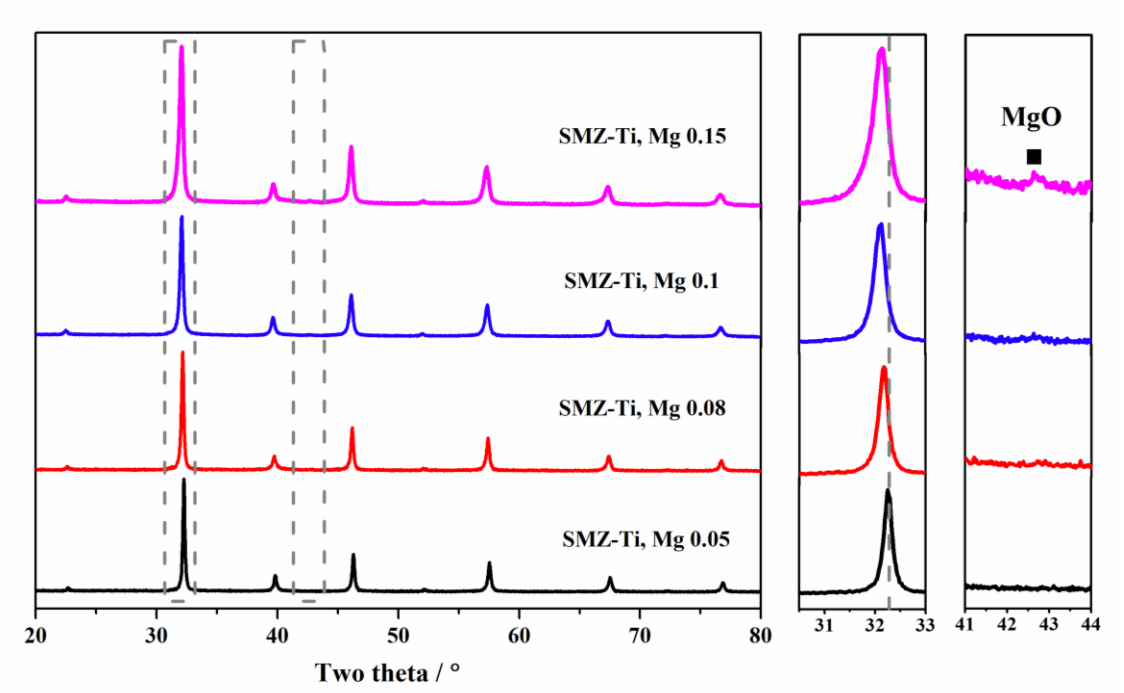

Figure S2. XRD patterns of SMZ-Ti oxides with different Mg content: $SrMg_xZr_{0.05}Ti_{0.95-x}O_{3-\delta}$ (SMZ-Ti, x= 0.05; 0.08, 0.1, 0.15) after calcinations at 950 ℃ for 10 h. (Related to Figure 1a)

Compared to $SrMg_{0.15}Zr_{0.05}Ti_{0.8}O_{3-\delta}$ consisted of a mixed dual phases (i.e. perovskite and MgO), all the other three titanates with lower Mg doping content, x = 0.05, 0.08 and 0.1, can be well crystallized with cubic perovskite structure without any additional phases. In addition, for low Mg contents ($x \leq 0.1$), the XRD peak shifts gradually towards smaller angles with increasing Mg content from x = 0.05 to 0.1, indicating the expansion of the unit cell since the ionic radius of Mg^{2+}(VI) (0.72 Å) is larger than those of Ti^{4+}. These results indicate that the solubility limit of Mg cation in $SrMg_xZr_{0.05}Ti_{0.95-x}O_{3-\delta}$ is higher than 0.1. These observations are in agreement with the results for $SrTi_{1-y}Mg_yO_3$ systems (Tkach et al., 2004). In the meanwhile, considering the benefits of Mg^{2+} ions doping for oxygen vacancy formation in SMZ-Ti, we selected $SrMg_{0.15}Zr_{0.05}Ti_{0.8}O_{3-\delta}$ to demonstrate its environment-induced mixed conductivity for coupling H_2O splitting with CH_4 reforming under low pO_2 atmospheres.

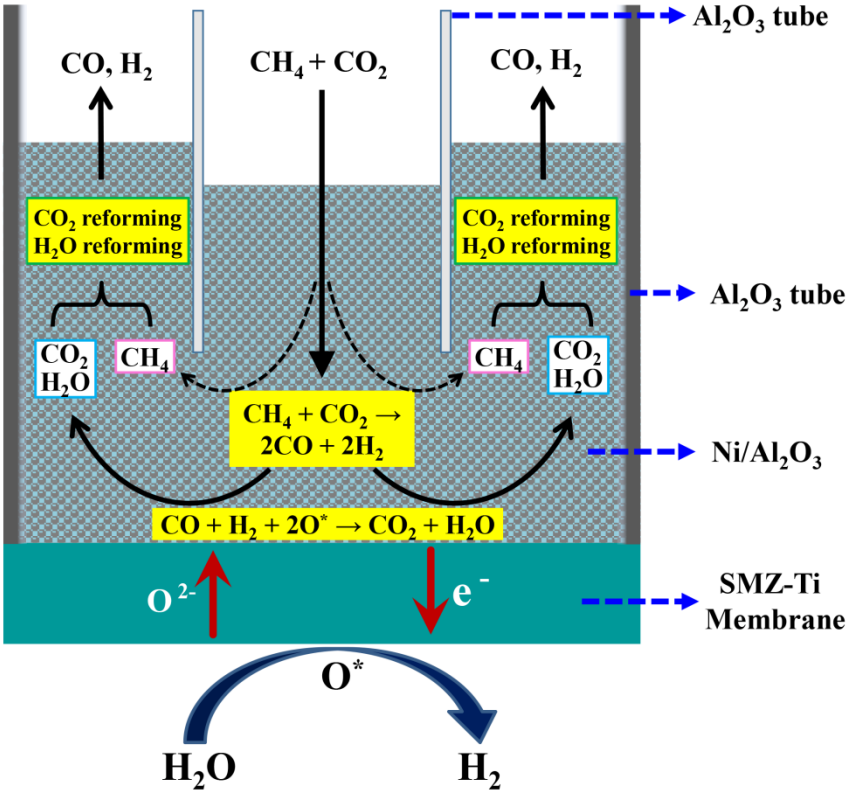

Figure S3. Scheme of catalytic reforming reactions taking place at the permeate side of SMZ-Ti membrane under Cond. IV. (Related to Figure 2)

As shown in Figure S3, before CH_4 and CO_2 reaching the membrane surface, dry reforming of methane with carbon dioxide ($CH_4 + CO_2 \rightarrow 2CO + 2H_2$) first takes place in the top zone of the catalyst, i.e. Ni/Al_2O_3. The generated syngas will further move to the membrane surface and be oxidized by the permeated oxygen on the membrane surface ($CO + H_2 + 2O^* \rightarrow H_2O + CO_2$). At the same time, part of the permeated oxygen may also be consumed by methane combustion according to POM reaction ($CH_4 + O^* \rightarrow CO + 2H_2$). The formed H_2O and CO_2 will leave from the membrane surface and react with the excess methane to produce syngas (CO_2 reforming and H_2O reforming) before leaving the catalyst bed.

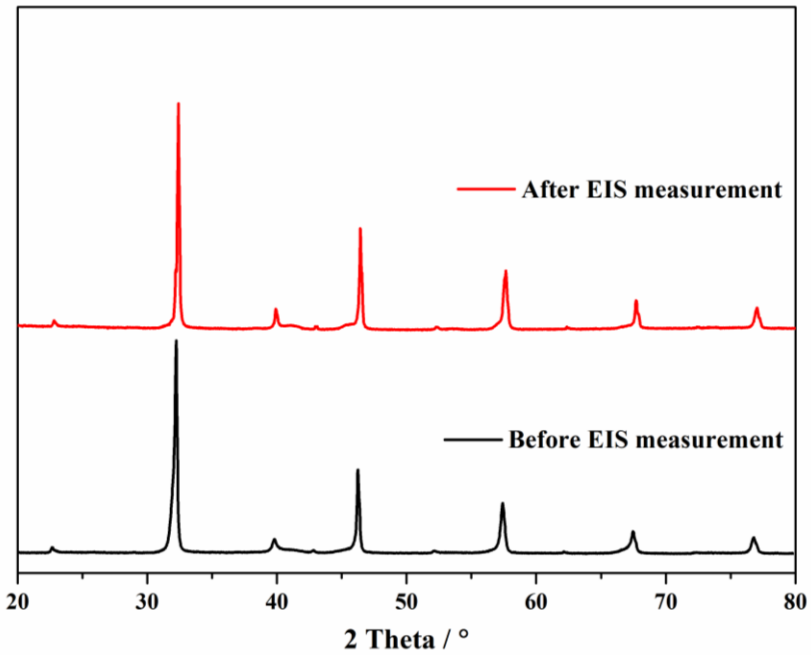

Figure S4. XRD pattern of SMZ-Ti membrane before and after electrical impedance spectroscopy (EIS) measurement for nearly 300 h. (Related to Figure 3)

Compared with the fresh membrane, no additional peaks of SMZ-Ti after electrical impedance spectroscopy (EIS) measurement was observed, which indicates the excellent redox stability of SMZ-Ti material in humidified H_2 and dry H_2 at high temperatures.

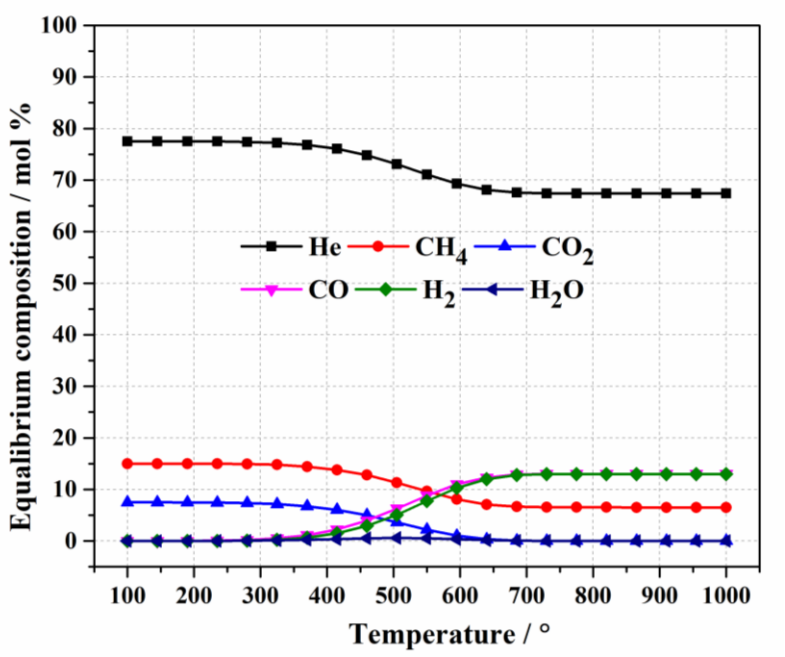

Figure S5. Thermodynamic equilibrium plots for DRM at 1 atm, from 100 – 1000 ℃ and at inlet feed compositions of 3 : 1.5 : 15.5 cm^3 min^{-1} of CH_4 : CO_2 : He, respectively. (Related to Figure 4a)

These plots were created by using Gibbs free energy minimization algorithm on HSC Chemistry 5.0 software. This calculation shows that the methane conversion at all temperature after 800 ℃ is constant for each case. Formation of H_2O by reverse water gas shift (RWGS) is not significant between 400 – 800 ℃, which is in agreement with the free energy calculations by Wang et al..(Wang et al., 1996) According to Figure S5, the equilibrium compositions of helium and methane (C_{He} and C_{CH_4}) at 990 ℃ are 67.4% and 6.52% respectively. So, the equilibrium methane conversion ($X_{CH_4,\ 990\ ℃}$) is 50.02 %.

$$X_{CH_4,\ 990\ ^\circ C} = \frac{F_{CH_4,\ feed} - \frac{F_{He}}{C_{He}} \times C_{CH_4}}{F_{CH_4,\ feed}} \times 100\% = \frac{3 - \frac{15.5}{0.674} \times 0.0652}{3} \times 100\% = 50.02\ \%$$

This methane conversion is lower than that using SMZ-Ti membrane reactor coupling water splitting with dry reforming of methane, suggesting that partial oxidation of methane (POM) may occur simultaneously with DRM in the SMZ-Ti membrane reactor.

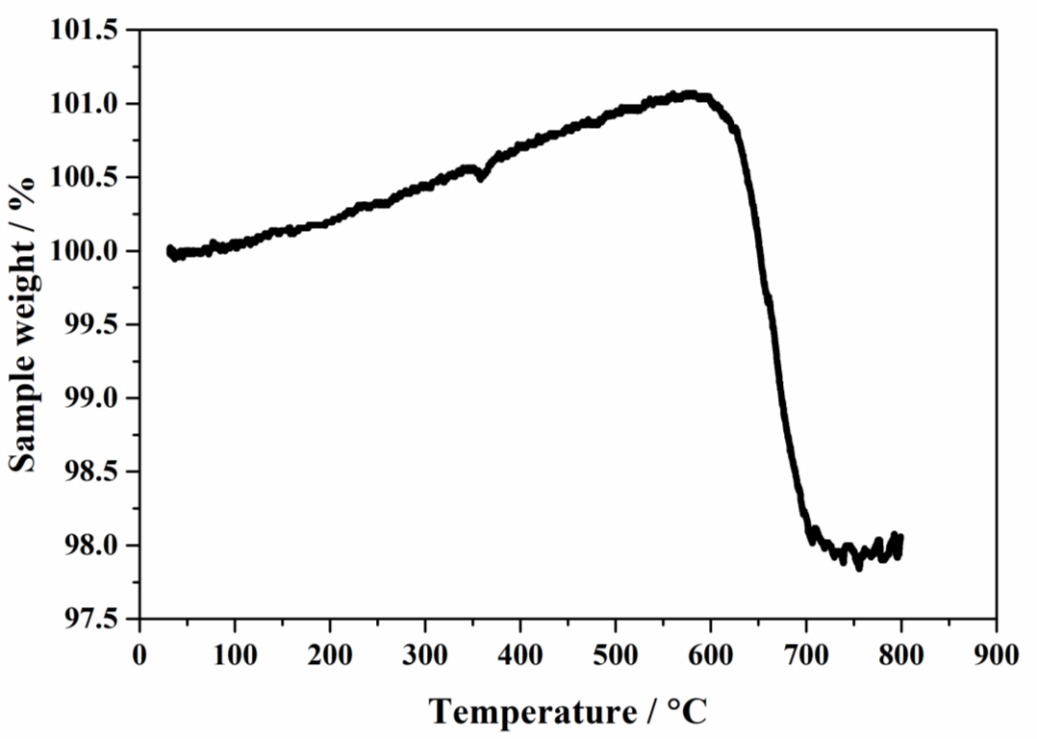

Figure S6. TGA behavior of the Ni/Al_2O_3 catalyst after the long-term methane reforming test. (Related to Figure 4a)

Similar to previous reports about TGA behaviors of spent Ni/Al_2O_3 catalyst (Zhou et al., 2015), an increase in the sample weight for the catalyst in the present work was observed at temperatures of 100 – 600 ℃ that could be due to the oxidation of Ni to nickel oxides. Higher than 600 ℃, the weight of the catalyst decreased quickly and became stable at approximately 98% at 800 ℃. Based on the TGA curve, the amount of deposited coke on the spent Ni/Al_2O_3 catalyst was only approximately 3.05 wt.%.

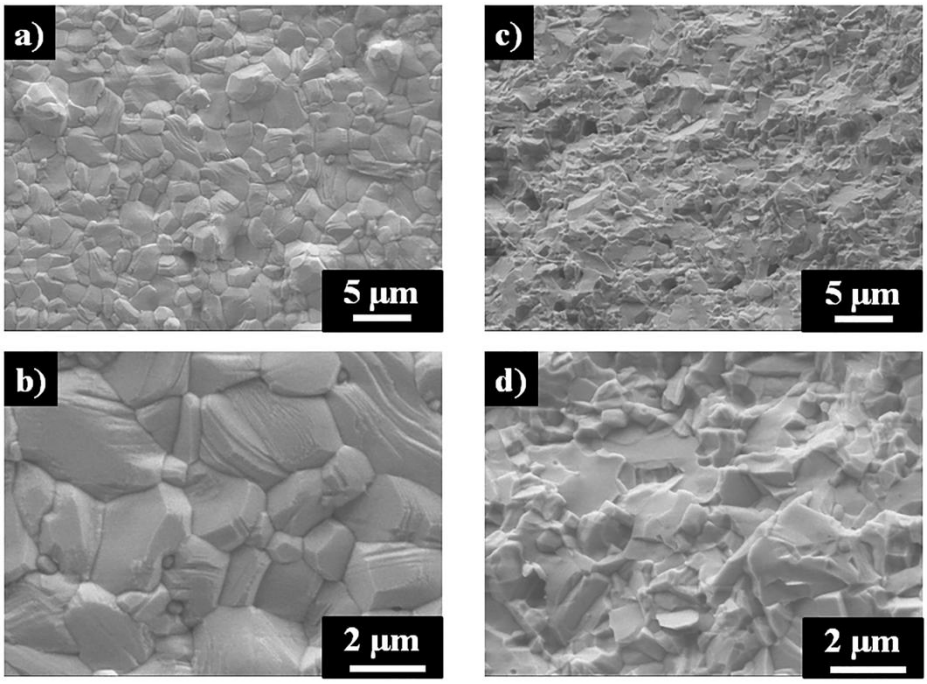

Figure S7 SEM images of as-prepared SMZ-Ti, where (a) and (b) are from surface view and (c) and (d) are from cross sectional views. (Related to Figure 4)

As shown in Figure S7, SMZ-Ti membrane is well sintered with large grains of 1 – 5 µm according to the surface morphology. From the cross-sectional view, the SMZ-Ti membrane was dense without pores.

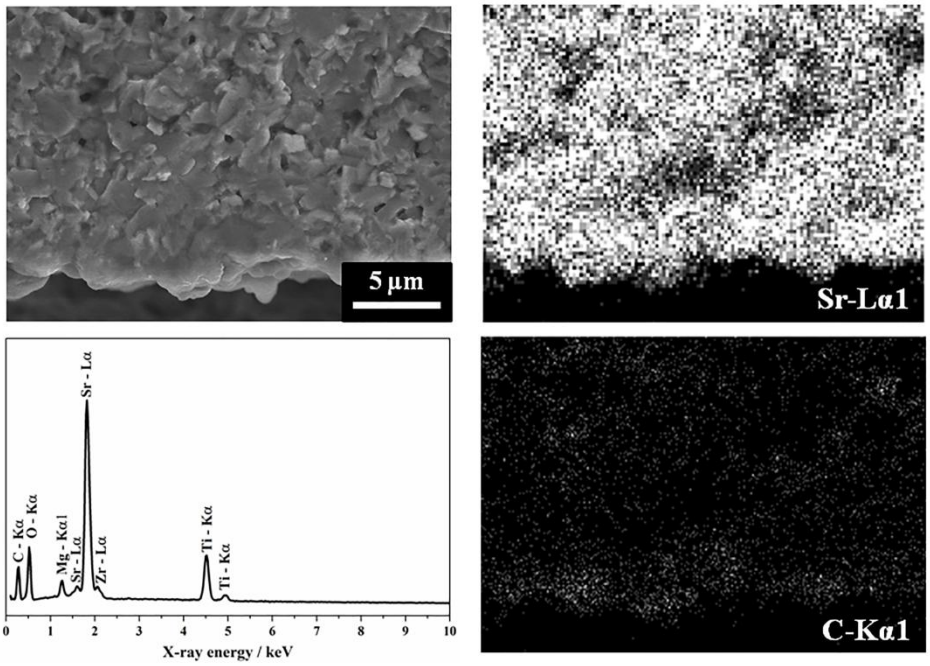

Figure S8. SEM image of the methane-carbon dioxide side of the SMZ-Ti membrane after long-term test for about 200 h, and the corresponding EDX elemental distributions of strontium and carbon. (Related to Figure 4)

As shown in Figure S8, no obvious enrichment of strontium and carbon along the fractured cross-section of the spent SMZ-Ti membrane was observed, indicating the SMZ-Ti membrane was not eroded by CO_2 during long-term exposure of methane and carbon dioxide at high temperature. In contrast, the performance of the cobalt and iron containing $SrCo_{0.4}Fe_{0.5}Zr_{0.1}O_{3-\delta}$ membrane reactor for coupling of POM with carbon dioxide decomposition was degraded seriously within 60 hours and the membrane broke significantly due to the erosion by the CO_2 and reducing atmospheres (Jin et al., 2008).

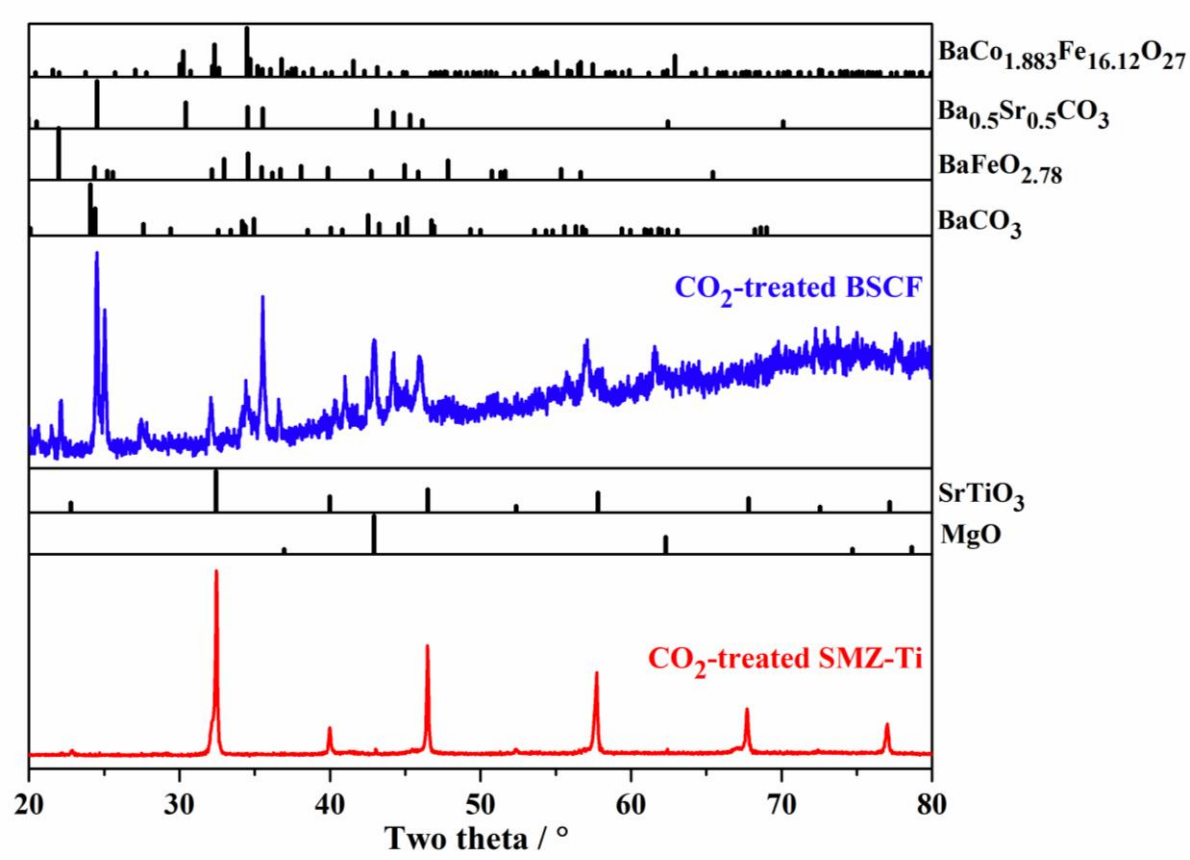

Figure S9. X-ray diffraction patterns of SMZ-Ti and BSCF annealed in 7.5 vol.% CO_2 in He at 990 ℃ for 24 h. (Related to Figure 4a)

According to the XRD results, the cubic structure of SMZ-Ti remained unchanged, and no carbonate formation was observed after the annealing. This observation is in contrast with that for $Ba_{0.5}Sr_{0.5}Co_{0.8}Fe_{0.2}O_{3-\delta}$ (BSCF), for which the perovskite structure has been partially or almost completely decomposed after exposure to CO_2 under the same condition. These results clearly demonstrate excellent CO_2 tolerance of SMZ-Ti.

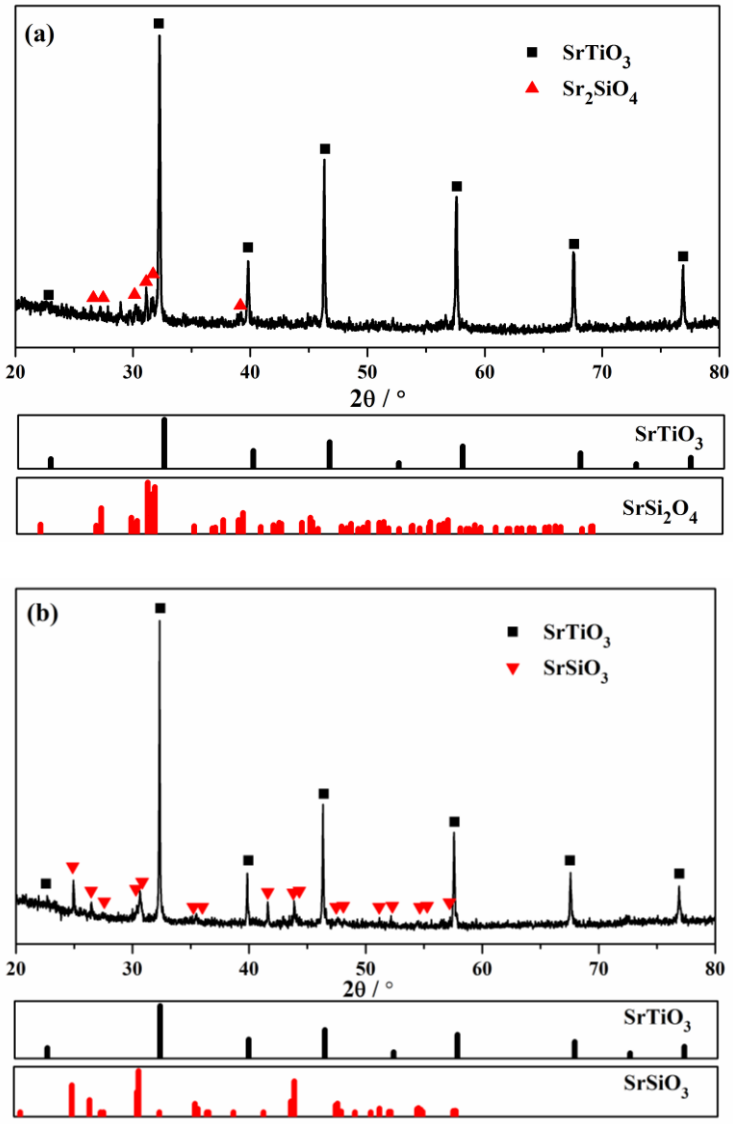

Figure S10 XRD patterns on the steam side (a) and the methane side (b) of spent SMZ-Ti membrane after coupling of water splitting and methane reforming. (Related to Figure 1a and Figure 4)

Figure S10 shows the XRD patterns of both side of the SMZ-Ti membrane after coupling process. Except the additional peaks of strontium silicate resulted from ceramic sealant at high temperature, the patterns either for steam side or methane side of spent SMZ-Ti membrane show no difference, which prove that SMZ-Ti membrane reactor are stable under reactions conditions.

Supporting Tables

Table S1. The equilibrium pO_2 at the two sides of SMZ-Ti membrane under four conditions. (Related to Figure 2)

		Gas composition for calculation	Equilibrium pO_2 at 990 ℃ / atm
Cond. I 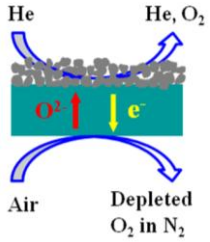	**Feed side**	N_2 (47.4 cm^3 min^{-1}) O_2 (12.59 cm^3 min^{-1})	0.21
	Permeate side	He (20 cm^3 min^{-1}), O_2 (0.012 cm^3 min^{-1})	6.20 x 10^{-4}
Cond. II 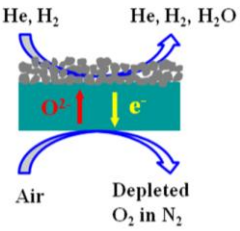	**Feed side**	N_2 (11.85 cm^3 min^{-1}) O_2 (3.07 cm^3 min^{-1})	0.204
	Permeate side	He (15 cm^3 min^{-1}), H_2 (5 cm^3 min^{-1}) O_2 (0.081 cm^3 min^{-1})	2.08 x 10^{-16}
Cond. III 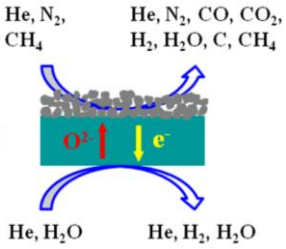	**Feed side**	He (10 cm^3 min^{-1}) H_2 (0.26 cm^3 min^{-1}) H_2O (29.74 cm^3 min^{-1})	2.45 x 10^{-9}
	Permeate side [a]	He (13 cm^3 min^{-1}), N_2 (4 cm^3 min^{-1}) CH_4 (3 cm^3 min^{-1}) O_2 (0.13 cm^3 min^{-1})	3.87 x 10^{-21}
Cond. IV 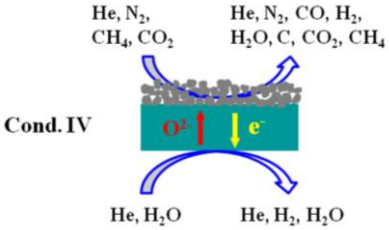	**Feed side**	He (10 cm^3 min^{-1}) H_2 (0.7 cm^3 min^{-1}) H_2O (29.3 cm^3 min^{-1})	3.34 x 10^{-10}
	Permeate side	He (11.5 cm^3 min^{-1}), N_2 (4 cm^3 min^{-1}) CH_4 (3 cm^3 min^{-1}) CO_2 (1.5 cm^3 min^{-1}) O_2 (0.35 cm^3 min^{-1})	2.03 x 10^{-19}

Table S1 shows the thermodynamic equilibrium pO_2 at 990 ℃ on the feed and permeate of SMZ-Ti membrane subjected to four different conditions at 1 atm. All the equilibrium composition on the two sides are calculated using Gibbs free energy minimization simulations using HSC Chemistry 5.0. Particularly in the case of condition III and condition IV, carbon formation at the permeate side even though not obvious, was taken into account due to the high CH_4/O_2 ratio of ~25 and CH_4 / CO_2 feed ratio of 2 at high temperature,(Mette et al., 2016; York et al., 2003) respectively.

Table S2. Exit gas composition and carbon balance as function of time of methane reforming into syngas via SMZ-Ti membrane reactor. (Related to Figure 4a)

Operating time / h	Composition (%)						Carbon balance $(X_{in}-X_{out})/X_{in}$ *100
	CH_4	CO_2	CO	H_2	He	N_2	
1	3.71	0.09	14.90	17.34	47.69	16.27	0.71
10	3.69	0.08	14.88	17.27	47.77	16.31	1.16
20	3.57	0.08	14.92	17.13	47.93	16.37	1.87
35	3.65	0.08	14.81	17.16	47.93	16.37	2.06
45	3.61	0.07	14.80	17.23	47.92	16.37	2.33
75	3.50	0.06	14.80	17.23	48.02	16.39	3.21

As shown in Table S2, the mole composition of the effluent stream at the permeate side of SMZ-Ti membrane reactor typically contains ~48 % He (carrier gas), ~16.3 % N_2 (internal standard gas in GC), ~3.6 % CH_4, ~17.2% H_2, ~14.9% CO and a small amount of CO_2 under H_2O / (CH_4-CO_2) partial pressure gradient at 990 ℃, revealing that the deep oxidation products H_2O and/or CO_2 are finally converted with unreacted CH_4 to syngas via reforming process. The carbon balances maintain over 96% within the investigation period. However, it is clear that the mole balance of carbon increased slowly with operating time, suggesting that slight carbon deposition may take place in the catalyst bed.

Transparent Methods

Synthesis

The $SrMg_{0.15}Zr_{0.05}Ti_{0.8}O_{3-\delta}$ (SMZ-Ti) membrane powders were synthesized by a combined citric acid and ethylenediaminetetraacetic acid (EDTA) method, as described in detail elsewhere.(Tong et al., 2003) Briefly speaking, stoichiometric amounts of $Sr(NO_3)_2$, $Mg(NO_3)_2$, and $ZrO(NO_3)_3$ powder were dissolved in de-ionized water, followed by the addition of EDTA and citric acid with EDTA: citric acid: total of metal cations molar ratio controlled at around 1: 1.5: 1. After agitation for a certain time, the pH value of the solution was adjusted to round 9 using ammonia solution to form solution A. Then, the stabilized titanium solution B consisting of proper amounts of tetrabutyl titanate ($Ti(OC_4H_9)_4$), ethanol (CH_3CH_2OH), acetic acid (CH_3COOH) and lactic acid ($CH_3CHOHCOOH$) was introduced into the solution A. The mixed solution was then heated at 120-150 ℃ for several hours under constant stirring to obtain a gel, which was calcined at 950 ℃ for 10 h to obtain SMZ-Ti powder with final composition. The resulting powders were uniaxially pressed at 10 MPa into disk membranes. Followed by the sintering of the green disks at 1450 ℃ in air for 10 h, dense SMZ-Ti membrane disks with thickness of 0.7 mm were obtained.

Similarly, the $SrMg_{0.05}Zr_{0.05}Ti_{0.9}O_{3-\delta}$, $SrMg_{0.08}Zr_{0.05}Ti_{0.87}O_{3-\delta}$, $SrMg_{0.1}Zr_{0.05}Ti_{0.85}O_{3-\delta}$, $La_{0.9}Ca_{0.1}FeO_{3-\delta}$ (LC-Fe), $SrTi_{0.75}Fe_{0.25}O_{3-\delta}$ (ST-Fe), $BaFe_{0.4}Zr_{0.2}Co_{0.4}O_{3-\delta}$ (BFZ-Co), $Ba_{0.98}Ce_{0.05}Fe_{0.95}O_{3-\delta}$ (BC-Fe), $Ce_{0.85}Sm_{0.15}O_{1.925}$ (75 wt.%) – $Sm_{0.6}Sr_{0.4}Al_{0.3}Fe_{0.7}O_{3-\delta}$ (25 wt.%) (SDC-SSAFe) and $Ba_{0.5}Sr_{0.5}Co_{0.8}Fe_{0.2}O_{3-\delta}$ (BSCF) membrane powders were also synthesized by the combined citric acid –EDTA method. All the powders were calcined at 950 ℃ for 10 h to crystallize well in cubic perovskite structures or cubic perovskite-fluorite structure.

For the deposition of SMZ-Ti porous layer onto the dense SMZ-Ti membrane, SMZ-Ti powders were first crushed well in a mortar, then several drops of distilled water were added to obtain SMZ-Ti paste. The paste was coated on one side of a SMZ-Ti membrane using a fine brush. The coated membranes were sintered at 1300 ℃ for 2 h in air with a heating and cooling rate of 3 ℃/min.

Electrical impedance measurement

The dense SMZ-Ti sample for impedance measurement was 1.03 mm thick with a diameter of 15.5 mm. Pt ink was sputtered onto both faces of the sample, and then fired at 1000 ˚C for 2 h.

Two-probe AC impedance spectroscopy of SMZ-Ti at 900 ℃ was performed using an Alpha-A high performance frequency analyzer (Novocontrol Technologies, Germeany) with a voltage amplitude of 40 mV and a frequency range spanning from 0.05 to 1 M Hz. The impedance was measured at 900 ℃ under atmospheres ranging from wet to dry H_2. Similar to previous studies,(Benisek et al., 2005; Lai et al., 2005) oxygen partial pressures lower than 0.21 atm were obtained using mixtures of Ar, H_2O and H_2, assuming a thermodynamic equilibrium between O_2, H_2 and H_2O. The oxygen partial pressure with H_2/H_2O ratio of 1, 10 and 30 at 900 ℃ calculated by HSC chemistry 5.0 are 4.9×10^{-15}, 4.9×10^{-17} and 5.5×10^{-18} atm, respectively. The total gas flow rates were fixed at 60 cm^3 min^{-1} using mass flow controllers. The whole system was allowed to stabilized under each condition before starting measurement. The typical stabilization time was over 50 h under low oxygen partial pressures atmospheres.

Membrane permeation performance

SMZ-Ti membrane pellet was sealed onto the alumina tube using commercial glass powders (Schott AG, Germany) and kept in the middle of an oven for isothermal conditions. The effective membrane area was 0.62 cm^2. The membrane reactor configuration was described elsewhere.(Cao et al., 2013) A Ni-based catalyst (0.3 g, Söd Chemie AG) was loaded on the SMZ-Ti porous layer of the membrane disk. The gas leakage of SMZ-Ti membrane at operating temperature was evaluated on the basis of our previous work (Liang et al., 2016). Basically, synthesized air and helium were introduced to the opposite sides of SMZ-Ti membrane. The concentrations of the effluent gas at helium side were measured online by a gas chromatograph (GC, Agilent 7890B). It is acceptable for permeation measurement when the amount of leakage oxygen is typically less than 5% of the total oxygen flux. Also, the gas leakage during the permeation measurement was on-line assessed by the leakage nitrogen from CH_4-CO_2 side to H_2O side of SMZ-Ti membrane.

After leakage test, two sides of SMZ-Ti membrane were successively exposed to four different conditions at 990 ℃ (i.e.: Air/He, Air/He-H_2, He-H_2O/CH_4-N_2-He, He-H_2O/CH_4-CO_2-N_2-He,) for oxygen permeation flux measurement. All the gas flow rates were controlled by gas mass-flow controllers (Bronkhorst). The H_2O flow was controlled by a liquid mass-flow controller (Bronkhorst) and completely evaporated at 160 ℃ before it was fed to the reactor. Also the lines from the outlets of products to the gas chromatograph were heated to 160 ℃. Gas composition was analyzed by an online gas chromatograph (GC, Agilent 7890B). The oxygen permeation fluxes were calculated from the amount of oxygen in the inlet and outlet streams on the air side

(Cond. I and Cond. II) or from the amount of generated hydrogen in the outlet streams on the steam side (Cond. III and Cond. IV).

Assuming that the oxygen from water splitting on the steam side under Cond. IV was totally removed and the total flow rate is constant, the hydrogen production rate on the steam side was calculated from the total flow rate F_{steam}(cm^3 min^{-1}), the hydrogen concentration c(H_2), and the effective membrane area S(cm^2) according to Equation (1). The CH_4 conversion X(CH_4) and the CO selectivity S(CO) on the methane-carbon dioxide side were calculated as Equations (2) and (3), where F(i) is the flow rate of species i on the methane-carbon dioxide side of the membrane.

$$J(H_2) = \frac{F_{steam}\, c(\mathrm{H_2})}{S} \tag{1}$$

$$X(CH_4) = (1 - \frac{F(CH_4, out)}{F(CH_4, in)}) \times 100\% \tag{2}$$

$$S(CO) = (\frac{F(CO)}{F(CH_4, in) + F(CO_2, in) - F(CH_4, out) - F(CO_2, out)}) \times 100\% \tag{3}$$

Thermal treatment

The pure SMZ-Ti, BFZ-Co, BC-Fe, SDC-SSAFe, LC-Fe and ST-Fe powders were treated in 20% H_2/Ar at 900 ℃ to prepare the H_2-exposed samples. Also, SMZ-Ti and synthesized BSCF powders were annealed in 7.5 vol. % CO_2 in helium at 990 ℃ for 24 h. 1.0 gram of BSCF powder was uniaxial pressed into green disk under 8 MPa. The green pellet was then sintered in air at 1130 ℃ for 10 h in muffle furnace. Afterwards, the BSCF membrane was treated under H_2/H_2O atmosphere (1 bar, 2.5 vol.% H_2, 75 vol.% H_2O, 22.5 vol. % He, total flow is 40 cm^3 min^{-1}) at 900 ℃ for 0.5 h.

Characterization

The crystal structures of SMZ-Ti, BFZ-Co, BC-Fe and SDC-SSAFe membrane powders were investigated by using a Bruker D8 ADVANCE diffractometer with a monochromator using Cu Kα radiation. Scanning electron microscopy (SEM) of SMZ-Ti and BSCF membranes was performed using a JEOL JSM-6700F field emission scanning electron microscope equipped with an ultrathin window Energy Dispersive X-ray detector to allow for elemental analysis. X-ray photoelectron spectroscopy (XPS) of SMZ-Ti membrane was performed on a PHI 5000 Versa Probe II (ULVAC-PHI, Inc) model X-ray photoelectron spectrometer instrument (AlKα radiation, $h\nu$ = 1.486 keV, 50 W) to analyze the surface of the sample before and after AC electrical impedance measurement. The binding energies (BE) were calibrated by setting the Ti 2p3 peak with the highest BE to 458.7 eV (Naumkin et al., 2012). The amount of carbon deposited on the catalyst was analyzed with TGA. The spent catalyst powder (10.288 mg) was placed in an alumina crucible and heated in flowing Air (rate: 50 cm^3 min^{-1}) at a heating rate of 5 K min^{-1} to 800 ℃, followed by cooling to room temperature.

Supplemental References

Benisek, A.,Sitte, W. (2005). Control of oxygen partial pressure by means of H_2–H_2O–O_2 or CO–CO_2–O_2 gas mixtures, J. Electrochem. Soc. *152*, H157-H160.

Cao, Z., Jiang, H., Luo, H., Baumann, S., Meulenberg, W.A., Assmann, J., Mleczko, L., Liu, Y., Caro, J. (2013). Natural gas to fuels and chemicals: Improved methane aromatization in an oxygen-permeable membrane reactor, Angew. Chem. Int. Ed. *52*, 13794-13797.

Jin, W., Zhang, C., Chang, X., Fan, Y., Xing, W., Xu, N. (2008). Efficient catalytic decomposition of CO_2 to CO and O_2 over Pd/mixed-conducting oxide catalyst in an oxygen-permeable membrane reactor, Environm. Sci. Tech. *42*, 3064-3068.

Lai, W.,Haile, S.M. (2005). Impedance spectroscopy as a tool for chemical and electrochemical analysis of mixed conductors: A case study of ceria, J. Am. Ceram. Soc. *88*, 2979-2997.

Liang, W., Megarajan, S.K., Liang, F., Zhang, Y., He, G., Liu, Z., Jiang, H. (2016). Coupling of N_2O decomposition with CO_2 reforming of CH_4 in novel cobalt-free $BaFe_{0.9}Zr_{0.05}Al_{0.05}O_{3-\delta}$ oxygen transport membrane reactor, Chem. Eng. J. *305*, 176-181.

Mette, K., Kühl, S., Tarasov, A., Willinger, M.G., Kröhnert, J., Wrabetz, S., Trunschke, A., Scherzer, M., Girgsdies, F., Düdder, H., Kähler, K., Ortega, K.F., Muhler, M., Schlögl, R., Behrens, M., Lunkenbein, T. (2016). High-temperature stable Ni nanoparticles for the dry reforming of methane, ACS Catal. *6*, 7238-7248.

Naumkin, A.V., Kraut-Vass, A., Gaarenstroom, S.W., Powell, C.J., NIST Standard Reference Database 20, *Version 4.1*. 2012.

Tkach, A., Vilarinho, P.M., Kholkin, A. (2004). Effect of Mg doping on the structural and dielectric properties of strontium titanate ceramics, Appl. Phys. A *79*, 2013-2020.

Tong, J., Yang, W., Cai, R., Zhu, B., Xiong, G., Lin, L. (2003). Investigation on the structure stability and oxygen permeability of titanium-doped perovskite-type oxides of $BaTi_{0.2}Co_xFe_{0.8-x}O_{3-\delta}$ (x=0.2–0.6), Sep. Purif. Tech. *32*, 289-299.

Wang, S., Lu, G.Q., Millar, G.J. (1996). Carbon dioxide reforming of methane to produce synthesis gas over metal-supported catalysts: State of the art, Energy & Fuels *10*, 896-904.

York, A.P.E., Xiao, T., Green, M.L.H. (2003). Brief overview of the partial oxidation of methane to synthesis gas, Top. Catal. *22*, 345-358.

Zhou, L., Li, L., Wei, N., Li, J., Basset, J.-M. (2015). Effect of $NiAl_2O_4$ formation on Ni/Al_2O_3 stability during dry reforming of methane, ChemCatChem *7*, 2508-2516.